Palladium(II) complexes of quinolinylaminophosphonates: synthesis, structural characterization, antitumor and antimicrobial activity

Journal of Inorganic Biochemistry 105 (2011) 867–879

Contents lists available at ScienceDirect

Journal of Inorganic Biochemistry

journal homepage: www.elsevier.com/locate/jinorgbio

Palladium(II) complexes of quinolinylaminophosphonates: Synthesis, structural characterization, antitumor and antimicrobial activity

Marina Juribašić [a], Krešimir Molčanov [a], Biserka Kojić-Prodić [a], Lisa Bellotto [b], Marijeta Kralj [c], Franca Zani [d], Ljerka Tušek-Božić [a,*]

[a] Division of Physical Chemistry, Ruđer Bošković Institute, Bijenička 54, HR-10002 Zagreb, Croatia
[b] CNR, Istituto di Scienze e Tecnologie Molecolari, Sezione di Padova, Corso Stati Uniti 4, 35100 Padova, Italy
[c] Division of Molecular Medicine, Ruđer Bošković Institute, Bijenička 54, HR-10002 Zagreb, Croatia
[d] Dipartimento Farmaceutico, Universitá degli Studi di Parma, 43124 Parma, Italy

ARTICLE INFO

Article history:
Received 30 September 2010
Received in revised form 16 March 2011
Accepted 16 March 2011
Available online 24 March 2011

Keywords:
Palladium(II) complex
Quinolinylaminophosphonate complex
Spectroscopy
Crystal structure
Antitumor activity
Antimicrobial activity

ABSTRACT

Three types of palladium(II) halide complexes of quinolinylaminophosphonates have been synthesized and studied. Diethyl and dibutyl [α-anilino-(quinolin-2-ylmethyl)]phosphonates (**L1, L2**) act as *N*,*N*-chelate ligands through the quinoline and aniline nitrogens giving complexes *cis*-[Pd(**L1/L2**)X_2] (X Cl, Br) (**1–4**). Their 3-substituted analogues [α-anilino-(quinolin-3-ylmethyl)]phosphonates (**L3, L4**) form dihalidopalladium complexes *trans*-[Pd(**L3/L4**)$_2X_2$] (**5–8**), with *trans N*-bonded ligand molecules only through the quinoline nitrogen. Dialkyl [α-(quinolin-3-ylamino)-*N*-benzyl]phosphonates (**L5, L6**) give tetrahalidodipalladium complexes [Pd_2(**L5/L6**)$_3X_4$] (**9–12**), containing one bridging and two terminal ligand molecules. The bridging molecule is bonded to the both palladium atoms, one through the quinoline and the other through the aminoquinoline nitrogen, whereas terminal ligand molecules are coordinated each only to one palladium *via* the quinoline nitrogen. Each palladium ion is also bonded to two halide ions in a *trans* square-planar fashion. The new complexes were identified and characterized by elemental analyses and by IR, UV–visible, ^{1}H, ^{13}C and ^{31}P nuclear magnetic resonance and ESI-mass spectroscopic studies. The crystal structures of complexes **1–4** and **6** were determined by X-ray structure analysis. The antitumor activity of complexes *in vitro* was investigated on several human tumor cell lines and the highest activity with cell growth inhibitory effects in the low micromolar range was observed for dipalladium complexes **11** and **12** derived from dibutyl ester **L6**. The antimicrobial properties *in vitro* of ligands and their complexes were studied using a wide spectrum of bacterial and fungal strains. No specific activity was noted. Only ligands **L3** and **L4** and tetrahalidodipalladium complexes **9** and **11** show poor activities against some Gram positive bacteria.

1. Introduction

Considerable research efforts have been made to develop novel metal-based antitumor complexes with the aim of improving effectiveness and reducing the severe side effects of the current clinical platinum chemotherapeutic agents such as cisplatin and its analogues [1,2]. The special attention has been directed to platinum complexes with different structural features than those of already used drugs [3–7] and complexes of the other platinum-group metals like ruthenium, rhodium, palladium and iridium [8–11]. Additionally, few complexes of other transition metals, like titanium, gallium and gold have also been found to be active and have entered clinical trials [10–12]. Recent studies on design of less toxic and more selective metal-based antitumor drugs are focused on complexes with biologically interesting ligands [10]. It is generally considered that the antitumor properties of complexes strongly depend on the nature of the ligands and the metal coordination pattern. With this regard, very interesting ligand candidates are derivatives of aminophosphonic acids owing to their broad-spectrum of biological activities and potential applications in the pharmacological and agrochemical fields [13–15]. With high affinity towards bone and other calcified tissues, these compounds may be utilized for drug design against bone diseases [16]. Our specific interest in the area of phosphonate chemistry has been directed towards dialkyl and monoalkyl esters of aromatic aminophosphonic acids and their complexes. Different types of palladium(II) and platinum(II) complexes with alkyl quinolinylmethylphosphonates and anilinobenzylphosphonates, such as molecular dihalide adducts with *trans* and *cis* configurations, mononuclear and binuclear metallocyclic and ion-pair halide salt complexes, have been synthesized, structurally characterized and screened on their antitumor and antiviral activity [17–24]. Some of these complexes demonstrated notable antitumor activity *in vitro* against some animal and human tumor cell lines, but showed no or only

* Corresponding author. Tel.: +385 1 4571217; fax: +385 1 4680245.
E-mail address: tusek@irb.hr (L. Tušek-Božić).

0162-0134/$ – see front matter © 2011 Elsevier Inc. All rights reserved.
doi:10.1016/j.jinorgbio.2011.03.011

marginal antiviral effects based on inhibition of virus-induced cytopathogenicity in various cell cultures.

The coordination chemistry of palladium(II) is very similar to that of platinum(II), but the higher liability in ligand exchange at Pd-centre (10^5-fold *vs* Pt) may cause rapid hydrolysis processes leading to dissociation of complex and formation of very reactive species unable to reach their biological targets. These problems could be overcome by using the bulky heterocyclic and chelating ligands. A number of palladium complexes with aromatic *N*- and *N*,*N*-containing ligands such as derivatives of pyridine, quinoline, pyrazole and 1,10-phenanthroline [9,25–27], as well as those with *N*,*S*-chelating ligands such as derivatives of thiosemicarbazones and dithiocarbamates, have shown very promising antitumor characteristics [28–30]. Some palladium(II) complexes exhibit significant antimicrobial activity [30]. In addition, quinoline moiety has pharmaceutical significance as important constituent in the structure of antimicrobial agents [31,32] and, recently, several quinoline phosphonates have been reported to be efficacious against bacteria and fungi [33].

Continuing our research program on preparation of metal complexes with dialkyl esters of various aromatic aminophosphonic acids with potential biological activity, in the present work we describe the synthesis, spectroscopic and biological properties of palladium(II) complexes with recently reported dialkyl quinolinylaminophosphonate (Fig. 1) [34,35]. Crystal structures of some palladium complexes were determined. Antimicrobial properties of free ligands and their complexes were studied *in vitro* on a wide spectrum of bacterial and fungal strains. The antiproliferative activity *in vitro* of complexes was investigated on a panel of human cell lines (T-lymphoblast leukemia cells and breast, colon and lung carcinoma). The results obtained were compared with those previously reported for palladium(II) halide complexes of quinolinylmethylphosphonates [19,24], and discussed with respect to their metal-binding behaviour and structure–activity relationships.

2. Experimental

2.1. General methods

All reagents and solvents were high purity products purchased from commercial sources and used without additional purification. The microwave (MW) irradiation experiments were carried out in sealed MW process vials (5 mL) with magnetic stirring using CEM Discover® LabmateTH/Explorer$_{PLS}$® monomode reactor. Melting points were determined on a hot stage microscope and are uncorrected. Infrared spectra were recorded on an ABB Bomem MB102 spectrometer using KBr (4000–400 cm^{-1}) and polyethylene (400–200 cm^{-1}) pellets. The one- and two-dimensional ^1H, ^{13}C and ^{31}P NMR spectra were recorded with Bruker XWIN-600 Fourier-transform spectrometer operating at 600.13 (and 300.13) MHz, 150.90 MHz and 242.92 MHz for ^1H, ^{13}C and ^{31}P nucleus, respectively. Spectra were recorded in $CDCl_3$ at 302 K (unless stated otherwise, at 253 and 323 K) containing $SiMe_4$ as an internal standard for ^1H and ^{13}C spectra or 85% H_3PO_4 as an external standard for ^{31}P spectra. The following techniques were used: ^1H, ^{13}C, APT, ^{31}P, ^1H-^1H COSY, ^1H-^{13}C HMQC, ^1H-^{13}C HMBC. All two-dimensional experiments were performed by standard pulse sequences, using Bruker XWINNMR software Version 3.5. The ESI mass spectrometric measurements were performed on a LCQDeca ion trap instrument (Thermo, San Jose, CA USA) operating in the positive ion mode. Compounds were dissolved in 1:1000 MeCN (**9–12**). The UV–vis spectra were obtained in chloroform solution with a HP Agilent 8453 diode array spectrophotometer in the 250–600 nm range. Conductance measurements were carried out at room temperature using a CD 7A Tacussel conductance bridge for 10^{-3} M solutions in DMF and methanol. Elemental analyses (C, H and N) were performed on a Perkin-Elmer Analyser PE 2400 Series 2 in the Ruđer Bošković Institute.

2.2. Synthesis of ligands

Diethyl and dibutyl [α-anilino-(quinolin-2-ylmethyl)]phosphonates (**L1, L2**), diethyl [α-anilino-(quinolin-3-ylmethyl)]phosphonate (**L3**) and diethyl and dibutyl [α-(quinolin-3-ylamino)-*N*-benzyl] phosphonates (**L5, L6**), prepared according to previously described methods [34,35], were purified by column chromatography performed on silica gel (130–270 mesh, 60 Å, Aldrich). New dibutyl [α-anilino-(quinolin-3-ylmethyl)]phosphonate (**L4**) was prepared by the same method under microwave irradiation.

Equimolar amounts of quinoline-3-carboxaldehyde (1.65 mmol) and aniline (1.65 mmol) were mixed and dibutyl phosphite in c.a. 10% molar excess (1.82 mmol) was added. Reaction mixture was quickly stirred, irradiated at max. 50 W for 10 min on 115 °C and chromatographed on

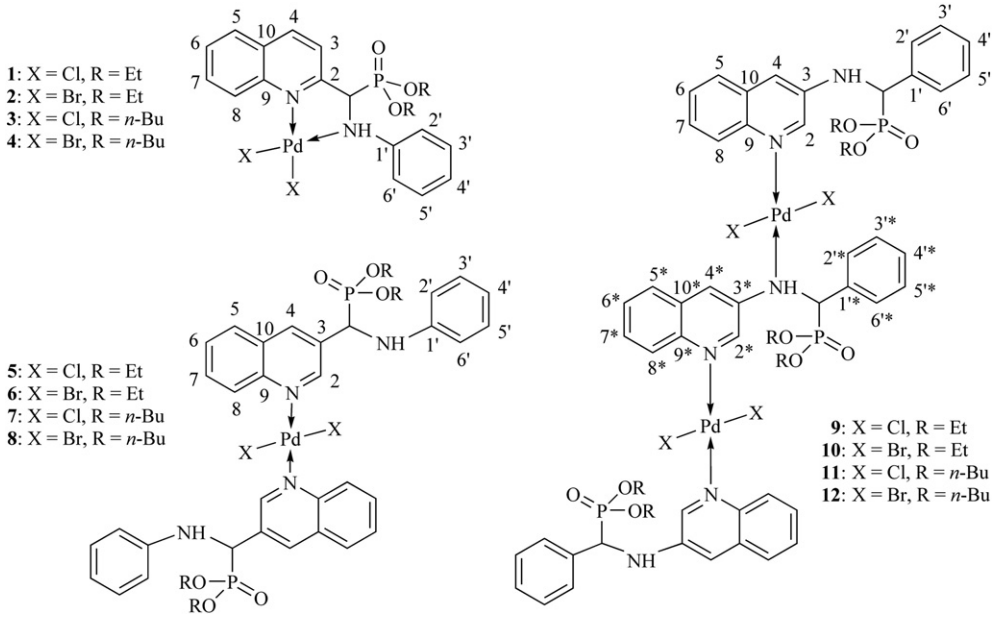

Fig. 1. Structures and numbering scheme of palladium(II) complexes with diethyl and dibutyl [α-anilino-(quinolin-2-ylmethyl)]phosphonate (**1–4**), diethyl and dibutyl [α-anilino-(quinolin-3-ylmethyl)]phosphonate (**5–8**) and diethyl and dibutyl [α-(quinolin-3-ylamino)-N-benzyl]phosphonate (**9–12**).

silica gel column using the mixture ethyl acetate:hexane = 2:1. Red-brown microcrystalline product **L4** was obtained by evaporation of the solvent *in vacuo*. Yield: 86%. M.p. 52–54 °C. Anal. Calc. for $C_{24}H_{31}N_2O_3P$: C, 67.59; H, 7.33; N 6.57%. Found: C, 67.42; H, 7.05; N, 6.66%.

2.3. Synthesis of complexes

2.3.1. General procedure for complexes cis-[PdLX$_2$] (**1–4**)

A solution of $Na_2[PdX_4]$ (X = Cl, Br 0.22 mmol) in methanol (2 mL) was added dropwise via micro syringe to a stirred solution of the ligand (L = **L1** or **L2**; 0.20 mmol) in methanol (2 mL). Microcrystalline red product precipitated immediately, and after stirring for 5 min was filtered off, washed with ice-cold methanol and dried *in vacuo* over P_2O_5. By prolonged stirring the initial red reaction mixture was slowly turned to ochre colour giving after a few days a mixture of the complexes, yellow aniline palladium dihalide adduct *trans*-[$Pd(PhNH_2)_2X_2$] (X = Cl, Br) [36] and grey *N,O*-chelate bis(quinolin-2-ylcarboxylato)palladium(II) complex [37].

*cis-[Pd(**L1**)Cl$_2$]* (**1**). Red solid. Yield: 77%. M.p. 180–183 °C. Anal. Calc. for $C_{20}H_{23}N_2O_3PCl_2Pd$: C, 43.86; H, 4.23; N, 5.11%. Found: C, 42.89; H, 4.22; N, 5.26%. IR (ν, cm^{-1}, vs—very strong, s—strong, m—medium, w—weak): 3206 w (ν(N–H)); 1594 m, 1512 m-s, 1493 m-s (ν(C=N), ν(C=C), δ(NH)); 1256 s, 1231 m (ν(P=O)); 1048 s, 1037 s, 1026 vs, 1010 vs (ν(PO–C)); 983 m-s, 973 m-s, 949 m, 930 w (ν(P–O–C), ν_{aliph}(C–C)); 340 m, 325 m (ν(Pd–Cl)). UV–vis (λ_{max}, nm (log(ε, $M^{-1}cm^{-1}$))): 316 (4.01), 328 (3.99), 405 (2.88). Crystals suitable for X-ray diffraction were grown by slow evaporation from the acetone solution at room temperature.

*cis-[Pd(**L1**)Br$_2$]* (**2**). Dark red solid. Yield: 82%. M.p. 166–168 °C. Anal. Calc. for $C_{20}H_{23}N_2O_3PBr_2Pd$: C, 37.73; H, 3.17; N, 4.40%. Found: C, 37.33; H, 3.72; N, 4.46%. IR (ν, cm^{-1}): 3211 w (ν(N–H)); 1594 m, 1511 m, 1493 m (ν(C=N), ν(C=C), δ(NH)); 1258 s, 1231 m (ν(P=O)); 1048 s, 1034 s, 1020 vs, 1009 s (ν(PO–C)); 973 m, 947 w-m, 928 w (ν(P–O–C), ν_{aliph}(C–C)); 288 w, 261 w (ν(Pd–Br)). UV–vis (λ_{max}, nm (log(ε, $M^{-1}cm^{-1}$))): 315 (4.08), 328 (4.07), 398 (3.08). Crystals suitable for X-ray diffraction were grown by slow evaporation from the acetone solution at room temperature. Single crystals of the acetonitrile monosolvate (**2**·MeCN) were obtained by slow evaporation from an acetonitrile solution in the refrigerator kept at +4 °C.

*cis-[Pd(**L2**)Cl$_2$]* (**3**). Orange-red solid. Yield: 71%. M.p. 166–168 °C. Anal. Calc. for $C_{24}H_{31}N_2O_3PCl_2Pd$: C, 47.74; H, 5.17; N, 4.64%. Found: C, 47.49; H, 5.11; N, 4.83%. IR (ν, cm^{-1}): 3206 w (ν(N–H)); 1596 m, 1513 m-s, 1493 m (ν(C=N), ν(C=C), δ(NH)); 1258 vs, 1232 m (ν(P=O)); 1061 m-s, 1026 vs, 1004 vs (ν(PO–C)); 977 s, 955 m, 928 w (ν(P–O–C), ν_{aliph}(C–C)); 340 m, 325 m (ν(Pd–Cl)). UV–vis (λ_{max}, nm (log(ε, $M^{-1}cm^{-1}$))): 316 (4.00), 328 (3.97), 405 (2.88). Crystals suitable for X-ray diffraction were grown by slow evaporation from an acetone or chloroform solution at room temperature.

*cis-[Pd(**L2**)Br$_2$]* (**4**). Red solid. Yield: 67%. M.p. 155–158 °C. Anal. Calc. for $C_{24}H_{31}N_2O_3PBr_2Pd$: C, 41.61; H, 4.51; N, 4.04%. Found: C, 41.45; H, 4.32; N, 3.93%. IR (ν, cm^{-1}): 3216 w (ν(N–H)); 1596 m, 1513 m, 1493 m (ν(C=N), ν(C=C), δ(NH)); 1258 vs, 1232 w-m (ν(P=O)); 1062 m-s, 1022 vs, 1003 s (ν(PO–C)); 975 s, 957 w-m, 926 w (ν(P–O–C), ν_{aliph}(C–C)); 284 w, 261 w (ν(Pd–Br)). UV–vis (λ_{max}, nm (log(ε, $M^{-1}cm^{-1}$))): 315 (4.07), 328 (4.05), 404 (3.08). Crystals suitable for X-ray diffraction were grown by slow evaporation of a solvent from the acetone or dichloromethane solution at room temperature or an acetonitrile solution in the refrigerator at +4 °C. The structure determination has been of limited accuracy, and the ORTEP view of the asymmetric unit is given in the Supplementary data.

2.3.2. General procedure for complexes trans-[PdL$_2$X$_2$] (**5–8**)

A solution of $Na_2[PdX_4]$ (X = Cl, Br; 0.11 mmol) in methanol (2 mL) and water (0.5 mL) was added dropwise avoiding any insolubilization to a stirred solution of the ligand (L = **L3** or **L4**; 0.20 mmol) in methanol (2 mL). After vigorous stirring for 3 h, the fine powder precipitate that formed was separated, washed with ice-cold methanol:water = 1:1 and dried *in vacuo* over P_2O_5.

*trans-[Pd(**L3**)$_2$Cl$_2$]* (**5**). Pale yellow solid. Yield: 95%. M.p. 139–142 °C. Anal. Calc. for $C_{40}H_{46}N_4O_6P_2Cl_2Pd$: C, 52.33; H, 5.05; N, 6.10%. Found: C, 51.56; H, 5.03; N, 6.34%. IR (ν, cm^{-1}): 3302 m (ν(N–H)); 1602 s, 1504 s (ν(C=N), ν(C=C), δ(NH)); 1240 s (ν(P=O)); 1047 vs, 1020 vs (ν(PO–C)); 971 m-s (ν(P–O–C), ν_{aliph}(C–C)); 350 w-m (ν(Pd–Cl)). UV–vis (λ_{max}, nm (log(ε, $M^{-1}cm^{-1}$))): 302 (4.16), 313 (4.15), 324 (4.11).

*trans-[Pd(**L3**)$_2$Br$_2$]* (**6**). Yellow solid. Yield: 90%. M.p. 158–160 °C. Anal. Calc. for $C_{40}H_{46}N_4O_6P_2Br_2Pd$: C, 47.71; H, 4.60; N, 5.56%. Found: C, 47.08; H, 4.64; N, 5.76%. IR (ν, cm^{-1}, sh-shoulder): 3293 m (ν(N–H)); 1602 s, 1503 s (ν(C=N), ν(C=C), δ(NH)); 1273 sh, 1265 sh, 1231 s (ν(P=O)); 1048 s, 1015 vs (ν(PO–C)); 966 m-s (ν(P–O–C), ν_{aliph}(C–C)); 299 w (ν(Pd–Br)). UV–vis (λ_{max}, nm (log(ε, $M^{-1}cm^{-1}$))): 301 (4.29), 313 (4.27), 325 (4.21). Crystals suitable for X-ray diffraction were grown by slow evaporation from an ethyl acetate (EtOAc) solution at room temperature.

*trans-[Pd(**L4**)$_2$Cl$_2$]* (**7**). Pale yellow solid. Yield: 95%. M.p. 193–194 °C. Anal. Calc. for $C_{48}H_{62}N_4O_6P_2Cl_2Pd$: C, 55.96; H, 6.07; N, 5.44%. Found: C, 55.90; H, 6.21; N, 5.53%. IR (ν, cm^{-1}): 3304 m (ν(N–H)); 1602 s, 1501 s (ν(C=N), ν(C=C), δ(NH)); 1268 sh, 1235 s (ν(P=O)); 1061 m-s, 1021 vs (ν(PO–C)); 990 vs, 958 sh (ν(P–O–C), ν_{aliph}(C–C)); 355 m (ν(Pd–Cl)). UV–vis (λ_{max}, nm (log(ε, $M^{-1}cm^{-1}$))): 302 (4.16), 313 (4.15), 324 (4.11).

*trans-[Pd(**L4**)$_2$Br$_2$]* (**8**). Yellow solid. Yield: 86%. M.p. 196–197 °C. Anal. Calc. for $C_{48}H_{62}N_4O_6P_2Br_2Pd$: C, 51.51; H, 5.58; N, 5.01%. Found: C, 51.34; H, 5.63; N, 5.06%. IR (ν, cm^{-1}): 3304 m (ν(N–H)); 1602 s, 1499 s (ν(C=N), ν(C=C), δ(NH)); 1267 w, 1235 s (ν(P=O)); 1061 m, 1021 s (ν(PO–C)); 989 s, 958 sh (ν(P–O–C), ν_{aliph}(C–C)); 299 w (ν(Pd–Br)). UV–vis (λ_{max}, nm (log(ε, $M^{-1}cm^{-1}$))): 301 (4.26), 313 (4.23), 325 (4.18).

2.3.3. General procedure for complexes [Pd$_2$L$_3$X$_4$] (**9–12**)

A solution of $Na_2[PdX_4]$ (X = Cl, Br; 0.15 mmol) in methanol (2 mL) was added dropwise to a stirred solution of the ligand (L = **L5** or **L6**; 0.20 mmol) in methanol (2 mL). Fine powder product precipitated immediately, and after stirring for 3 h was filtered off, washed with ice-cold methanol and dried *in vacuo* over P_2O_5.

*[Pd$_2$(**L5**)$_3$Cl$_4$]* (**9**). Pale yellow solid. Yield: 86%. M.p. >200 °C decomp. Anal. Calc. for $C_{60}H_{69}N_6O_9P_3Cl_4Pd_2$: C, 50.33; H, 4.96; N, 5.87%. Found: C, 50.09; H, 5.11; N, 5.89%. IR (ν, cm^{-1}, br—broad): 3267 m-s br (ν(N–H)); 1619 s, 1609 s, 1541 m, 1493 m (ν(C=N), ν(C=C), δ(NH)); 1239 s, 1223 vs (ν(P=O)); 1048 vs, 1018 vs (ν(PO–C)); 975 s (ν(P–O–C), ν_{aliph}(C–C)); 348 w-m (ν(Pd–Cl)). UV–vis (λ_{max}, nm (log(ε, $M^{-1}cm^{-1}$))): 260 (4.92), 308 (3.92), 368 (4.24). ESI MS: *m/z* 1489 (8%), $[M+Na]^+$; 1118 (19%), $[(M+Na)\text{-}L]^+$; 941 (95%), $[(M+Na)\text{-}PdLCl_2]^+$; 571 (11%), $[(M+Na)\text{-}PdL_2Cl_2]^+$; 535 (23%), $[(M+Na)\text{-}PdL_2Cl_2\text{-}HCl]^+$; 393 (9%) $[(M+Na)\text{-}Pd_2L_2Cl_4]^+ = [L+Na]^+$.

*[Pd$_2$(**L5**)$_3$Br$_4$]* (**10**). Ochre solid. Yield: 82%. M.p. >200 °C decomp. Anal. Calc. for $C_{60}H_{69}N_6O_9P_3Br_4Pd_2$: C, 44.16; H, 4.35; N, 5.15%. Found: C, 44.38; H, 4.41; N, 5.72%. IR (ν, cm^{-1}): 3266 m br (ν(N–H)); 1617 s, 1609 s, 1543 w-m, 1493 m (ν(C=N), ν(C=C), δ(NH)); 1239 s, 1223 vs (ν(P=O)); 1048 vs, 1022 vs (ν(PO–C)); 975 m-s (ν(P–O–C), ν_{aliph}(C–C)); 292 w (ν(Pd–Br)). UV–vis (λ_{max}, nm (log(ε, $M^{-1}cm^{-1}$))): 257 (5.05), 311 (4.13), 368 (4.26). ESI MS: *m/z* 1667 (<1%), $[M+Na]^+$; 1296 (9%), $[(M+Na)\text{-}L]^+$; 1030 (100%), $[(M+Na)\text{-}PdLBr_2]^+$; 660 (23%), $[(M+Na)\text{-}PdL_2Br_2]^+$; 579 (32%), $[(M+Na)\text{-}PdL_2Br_2\text{-}HBr]^+$; 393 (19%) $[(M+Na)\text{-}Pd_2L_2Br_4]^+ = [L+Na]^+$.

*[Pd$_2$(**L6**)$_3$Cl$_4$]* (**11**). Pale yellow solid. Yield: 77%. M.p. >200 °C decomp. Anal. Calc. for $C_{72}H_{93}N_6O_9P_3Cl_4Pd_2$: C, 52.92; H, 5.74; N, 5.14%. Found: C, 54.20; H, 6.12; N, 5.36%. IR (ν, cm^{-1}): 3273 m br (ν(N–H)); 1618 s, 1609 s, 1542 m, 1493 m (ν(C=N), ν(C=C), δ(NH)); 1240 s, 1222 s (ν(P=O)); 1063 s, 1022 vs (ν(PO–C)); 994 vs (ν(P–O–C), ν_{aliph}(C–C)); 348 w-m (ν(Pd–Cl)). UV–vis (λ_{max}, nm (log(ε, $M^{-1}cm^{-1}$))):

260 (4.91), 308 (3.97), 369 (4.23). ESI MS: *m/z* 1657 (7%), $[M+Na]^+$; 1231 (15%), $[(M+Na)\text{-}L]^+$; 1053 (100%), $[(M+Na)\text{-}PdLCl_2]^+$; 627 (10%), $[(M+Na)\text{-}PdL_2Cl_2]^+$; 591 (15%), $[(M+Na)\text{-}PdL_2Cl_2\text{-}HCl]^+$; 449 (27%) $[(M+Na)\text{-}Pd_2L_2Cl_4]^+ = [L+Na]^+$.

$[Pd_2(\mathbf{L6})_3Br_4]$ (**12**). Yellow solid. Yield: 82%. M.p. >200 °C decomp. Anal. Calc. for $C_{72}H_{93}N_6O_9P_3Br_4Pd_2$: C, 48.04; H, 5.29; N, 4.67%. Found: C, 48.33; H, 5.57; N, 4.83%. IR (ν, cm^{-1}): 3268 m br (ν(N–H)); 1618 s, 1608 s, 1543 w-m, 1493 m (ν(C=N), ν(C=C), δ(NH)); 1240 s, 1222 vs (ν(P=O)); 1062 m, 1023 vs (ν(PO–C)); 993 s (ν(P–O–C), ν_{aliph}(C–C)); 289 w (ν(Pd–Br)). UV–vis (λ_{max}, nm ($\log(\varepsilon, M^{-1}cm^{-1})$)): 257 (5.05), 311 (4.11), 369 (4.25). ESI MS: *m/z* 1835 (5%), $[M+Na]^+$; 1408 (5%), $[(M+Na)\text{-}L]^+$; 1142 (100%), $[(M+Na)\text{-}PdLBr_2]^+$; 716 (17%), $[(M+Na)\text{-}PdL_2Br_2]^+$; 635 (33%), $[(M+Na)\text{-}PdL_2Br_2\text{-}HBr]^+$; 449 (15%) $[(M+Na)\text{-}Pd_2L_2Br_4]^+ = [L+Na]^+$.

2.4. X-ray structure analysis

Single crystals of **1–4** and **6** were measured on an Oxford Diffraction Xcalibur Nova R diffractometer (microfocus Cu tube, CCD detector). Program package CrysAlis PRO [38] was used for data reduction. The structures were solved using SHELXS97 and refined with SHELXL97 [39]. The models were refined using the full-matrix least squares refinement; all non-hydrogen atoms were refined anisotropically. Hydrogen atoms (except NH) were treated as constrained entities, using the command AFIX in SHELXL97 [39]. Molecular geometry calculations were performed by PLATON [40] and the molecular graphics were prepared using ORTEP-3 [41] and CCDC-Mercury [42]. Crystallographic and refinement data for the structures reported in this paper are shown in Table 1.

Crystallographic data for the structural analysis have been deposited with the Cambridge Crystallographic Data Centre, CCDC No. 794995-795000. The data can be obtained free of charge *via* www.ccdc.cam.ac.uk/conts/retrieving.html, or from the Cambridge Crystallographic Data Centre, 12, Union Road, Cambridge CB2 1EZ, UK; fax: +44 1223 336033; or deposit@ccdc.cam.ac.uk.

2.5. Antitumor evaluation assays

The experiments were carried out on five human cell lines, which are derived from four cancer types. The following cell lines were used: SW 620 and HCT 116 (colon carcinoma), H 460 (lung carcinoma), MCF-7 (breast carcinoma) and MOLT-4 (T-lymphoblast leukemia). The cells were cultured as monolayers and maintained in Dulbecco's modified Eagle's medium (DMEM) supplemented with 10% fetal bovine serum (FBS), 2 mM L-glutamine, 100 U/ml penicilin and 100 mg/mL streptomycin in a humidified atmosphere with 5% CO_2 at 37 °C.

The growth inhibition activity was assessed according to the slightly modified procedure performed at the National Cancer Institute, Developmental Therapeutic Program [43]. The panel cell lines were inoculated onto a series of standard 96-well microtiter plates on day 0, at 1×10^4 to 3×10^4 cells/mL, depending on the doubling times of specific cell line. Test agents were then added in five- or ten-fold dilutions (10^{-8} to 10^{-4} M) and incubated for further 72 h. Working dilutions were freshly prepared on the day of testing. The solvent (DMSO) was also tested for eventual inhibitory activity by adjusting its concentration to be the same as in working concentrations. After 72 h of incubation the cell growth rate was evaluated by performing the MTT assay [44], which detects dehydrogenase activity in viable cells. The absorbance (OD, optical density) was measured on a microplate reader at 570 nm. The absorbance is directly proportional to the number of living, metabolically active cells [44]. The percentage of growth (PG) of the cell lines was calculated according to one or the other of the following two expressions.

If $(\text{mean OD}_{test} - \text{mean OD}_{tzero}) \geq 0$, then $PG = 100\times(\text{mean OD}_{test} - \text{mean OD}_{tzero})/(\text{mean OD}_{ctrl} - \text{meanOD}_{tzero})$. If $(\text{mean OD}_{test} - \text{mean OD}_{tzero}) < 0$, then: $PG = 100\times(\text{mean OD}_{test} - \text{mean OD}_{tzero})/OD_{tzero}$,

Table 1
Crystallographic data, collection and structure refinement data of complexes **1–4** and **6**.

Complex	**1**	**2**	**2**·MeCN	**3**	**4**	**6**·2EtOAc
Empirical formula	$C_{20}H_{23}Cl_2N_2O_3PPd$	$C_{20}H_{23}Br_2N_2O_3PPd$	$C_{22}H_{26}Br_2N_3O_3PPd$	$C_{24}H_{31}Cl_2N_2O_3PPd$	$C_{24}H_{31}Br_2N_2O_3PPd$	$C_{48}H_{62}Br_2N_4O_{10}P_2Pd$
Formula weight	547.67	636.59	677.63	603.78	692.68	1183.16
Crystal dimensions/mm	0.23×0.13×0.06	0.20×0.15×0.10	0.15×0.12×0.10	0.15×0.09×0.07	0.15×0.12×0.10	0.16×0.14×0.11
Colour	Light red	Red	Red	Orange	Red	Yellow
Solvent used for crystallization	Acetone	Acetone	MeCN	Acetone, $CHCl_3$	Acetone, CH_2Cl_2, MeCN	EtOAc
Space group	$P\,2_12_12_1$	$P\,2_1/c$	$P\,2_1/n$	$P\,2_1/c$	$P\,2_1/c$	$P\,\bar{1}$
a/Å	15.4282(1)	10.6650(1)	9.44584(6)	10.1639(1)	27.0301(9)	9.3411(4)
b/Å	16.0030(1)	15.8511(2)	15.47859(10)	12.6778(1)	18.0654(5)	9.7802(4)
c/Å	18.4946(1)	14.6300(2)	18.10265(12)	20.3398(2)	22.8664(7)	14.9894(5)
α/°	90	90	90	90	90	97.122(3)
β/°	90	110.284(1)	104.7280(7)	95.803(1)	105.803(3)	94.837(3)
γ/°	90	90	90	90	90	93.570(9)
Z	8	4	4	4	16	1
V/Å^3	4566.27(5)	2319.86(5)	2559.80(3)	2607.47(4)	10743.9(6)	1350.33(9)
D_{calc}/g cm^{-3}	1.593	1.823	1.758	1.538	1.713	1.455
μ/mm^{-1}	9.571	11.337	10.330	8.437	9.846	5.528
Absorption correction	Multi-scans	Multi-scans	Multi-scans	Multi-scans	Multi-scans	Multi-scans
T_{min}, T_{max}	0.462, 1.000	0.124, 0.322	0.489, 1.000	0.352, 0.550	0.295, 1.000	0.405, 0.544
Θ range/°	3.65–76.21	4.26–76.55	3.81–76.15	4.11–77.42	2.44–76.57	2.98–75.00
Range of *h*, *k*, *l*	$18\geq h\geq -18$	$13\geq h\geq -13$	$11\geq h\geq -11$	$12\geq h\geq -12$	$30\geq h\geq -33$	$11\geq h\geq -11$
	$20\geq k\geq -18$	$19\geq k\geq -19$	$18\geq k\geq -19$	$15\geq k\geq -15$	$21\geq k\geq -21$	$12\geq k\geq -10$
	$22\geq l\geq -23$	$18\geq l\geq -18$	$21\geq l\geq -22$	$23\geq l\geq -25$	$24\geq l\geq -28$	$18\geq l\geq -15$
Reflections collected	15,786	22,070	13,211	26,496	49,100	11,764
Independent reflections	7748	4338	4836	4844	14,282	4864
Observed reflections ($I\geq 2\sigma$)	8163	4812	5301	5402	21,488	5483
R_{int}	0.0197	0.0327	0.0191	0.0375	0.0546	0.0239
R (F)	0.0296	0.0286	0.0259	0.0341	0.0925	0.0429
R_w (F^2)	0.0804	0.0819	0.0713	0.0973	0.3150	0.1405
Goodness of fit	1.052	1.051	1.053	1.082	1.046	1.220
No. of parameters	613	294	331	317	1413	382
F(000)	2208.0	1248.0	1336.0	1232.0	5504.0	604.0
$\Delta\rho_{max}$, $\Delta\rho_{min}$ (eÅ^{-3})	0.520, −0.740	0.978, −0.913	0.431, −0.564	0.787, −0.603	1.385, −1.471	1.082, −0.840

where the mean OD_{tzero} is the average of optical density measurements before exposure of cells to the test compound, the mean OD_{test} is the average of optical density measurements after the desired period of time and the mean OD_{ctrl} is the average of optical density measurements after the desired period of time with no exposure of cells to the test compound.

Each test was performed in quadruplicate in three individual experiments. The results are expressed as IC_{50}, which is the concentration necessary for 50% of inhibition. The IC_{50} values for each compound are calculated from concentration–response curves using linear regression analysis by fitting the test concentrations that give PG values above and below the reference value (*i.e.* 50%). If however, for a given cell line all of the tested concentrations produce PGs exceeding the respective reference level of effect (*e.g.* PG value of 50), then the highest tested concentration is assigned as the default value, which is preceded by a ">" sign. Each result is a mean value from three separate experiments.

2.6. Antimicrobial activity

The antimicrobial activity of the synthesized compounds was examined *in vitro* against ten Gram positive bacteria (*Bacillus megaterium* BGSC 7A2, *Bacillus subtilis* ATCC 6633, *Bacillus thuringiensis* var. *kurstaki* BGSC 4D1, *Sarcina lutea* ATCC 9341, *Staphylococcus aureus* ATCC 6538, *Staphylococcus epidermidis* ATCC 12228 and clinical isolates of *Staphylococcus haemolyticus*, *Streptococcus agalactiae*, *Streptococcus faecalis*, *Streptococcus faecium*), eight Gram negative bacteria (*Enterobacter cloacae* ATCC 23355, *Escherichia coli* ATCC 8739, *Haemophilus influenzae* ATCC 19418, *Proteus vulgaris* ATCC 13315, *Pseudomonas aeruginosa* ATCC 9027, *Salmonella typhimurium* ATCC 14028, *Serratia marcescens* ATCC 8100, a clinical isolate of *Klebsiella pneumoniae*), two yeasts (*Candida tropicalis* ATCC 1369, *Saccharomyces cerevisiae* ATCC 9763) and a mould (*Aspergillus niger* ATCC 6275). The two-fold broth dilution technique [45] was used. The minimal inhibitory concentrations (MIC, μg/mL) were defined as the lowest concentrations of compound required to give complete inhibition of the growth of each strain. All compounds were dissolved in DMSO, then added to nutrient media (Haemophilus Test Medium for *H. influenzae*, Mueller Hinton Broth for other bacteria and Sabouraud Liquid Medium for fungi) to obtain final concentrations ranging from 1.5 μg/mL to 200 μg/mL. The amount of DMSO never exceeded 1% v/v. Inoculum size was 5×10^5 bacteria/mL and 1×10^3 fungi/mL. The MICs were read after incubation at 37 °C for 24 h (bacteria) and at 30 °C for 48 h (fungi). Media and media with 1% v/v DMSO were employed as growth controls. Ciprofloxacin and miconazole were used as standard antibacterial and antifungal drugs, respectively.

To detect the minimum bactericidal concentrations (MBC, μg/mL), 100 μL of liquid from each suspension remaining clear were subcultured in fresh medium and the samples were incubated at 37 °C for 24 h. MBC values represent the lowest concentration of drug needed for the reduction of the initial inoculum of 99.9%.

All experiments were performed in triplicate and repeated at least three times.

3. Results and discussion

3.1. Synthesis and properties

All three types of quinoline-based aminophosphonate ligands contain three potential donor atoms, quinoline nitrogen, aniline or aminoquinoline nitrogen and phosphoryl oxygen, but their reaction with $Na_2[PdCl_4]$ (X=Cl, Br) in methanol afforded formation of complexes with different metal–ligand interactions (Fig. 1). Their structure was defined by elemental analysis, conductance measurements, X-ray single-crystal diffraction and various spectroscopic methods (IR, multinuclear NMR, UV–visible, ESI MS). It was found that dialkyl [α-anilino-(quinolin-2-ylmethyl)]phosphonates (**L1, L2**) act as bidentate ligands through the quinoline and aniline nitrogens giving complexes *cis*-[Pd(**L1**/**L2**)X_2] (**1–4**) with the five-membered *N,N*-chelate ring and which was supported by their X-ray analysis. These complexes were isolated immediately after their formation, *i.e.* after about 5 min of stirring the reactants, while prolonged stirring caused their slow decomposition and the formation of a mixture of complexes, which were detected as an aniline palladium dihalide adduct *trans*-[Pd$(PhNH_2)_2X_2$] (X=Cl, Br) [36] and *N,O*-chelate bis(quinolin-2-ylcarboxylato)palladium(II) complex [37], confirmed by the spectroscopic and X-ray crystallographic studies. It is interesting to note that in the microwave-assisted synthesis of **L1** and **L2** by one-pot three-component reaction of quinoline-2-carboxaldehyde, aniline and dialkyl phosphite, as the main product was isolated quinoline-2-carboxanilide and not dialkyl phosphonates as in the conventional thermal reaction [34]. Favoured formation of amide, and not of required imine, by reaction of quinoline-2-carboxaldehyde and aniline may arise from proximity of the acidic aldehyde hydrogen with respect to the quinoline nitrogen.

The 3-substituted quinoline analogues, dialkyl [α-anilino-(quinolin-3-ylmethyl)]phosphonates (**L3, L4**) form dihalidopalladium complexes with 1:2 metal-to-ligand ratio, *trans*-[Pd(**L3**/**L4**)$_2X_2$] (**5–8**), containing *trans N*-bonded ligand molecules only through the quinoline nitrogen. It is unlikely that such bulky two phosphonate ligand molecules could be placed in *cis* position with respect to the metal ion as well as it may be presumed that the steric effects inhibit the aniline nitrogen coordination and 1:1 metal-to-ligand chelate formation as was obtained in the complexes **1–4**. The coordination behaviour of these ligands was supported by the X-ray analysis of complex **6**. The situation is more complicated in the case of dialkyl [α-(quinolin-3-ylamino)-*N*-benzyl] phosphonates (**L5, L6**), which give tetrahalidodipalladium complexes, [Pd_2(**L5**/**L6**)$_3X_4$] (**9–12**) containing three ligand molecules. A bridging molecule is bonded to the both palladium atoms, one through the quinoline nitrogen and the other through the aminoquinoline nitrogen. The two other terminal ligand molecules are coordinated each only to one palladium *via* the quinoline nitrogen and each palladium ion is also bonded to two halide ions in a *trans* square-planar fashion. It could be concluded that the geometric and steric requirements of the ligand containing two or more donor atoms are very important in determining the number of donor atoms that will coordinate and the final geometry of the metallic species.

The novel complexes prepared are microcrystalline or powder-like diamagnetic compounds, coloured yellow to dark-red, and they are stable in the solid state under normal laboratory conditions. From the very low molar conductance in DMF and methanol solutions (<10 S cm^2 mol^{-1}) it may be concluded that these complexes are true molecular addition compounds. In general, all the complexes are insoluble in water and soluble or slightly soluble in a number of common organic solvents. The complexes **1–4** are the most soluble whereas complexes **9–12** are the least soluble compounds. Elemental and spectroscopic (IR, NMR, MS) analyses of complexes clearly confirm the 1:1, 1:2 and 2:3 metal-to-ligand ratio in complexes **1–4**, **5–8** and **9–12**, respectively. It is worth mentioning that the great similarity in the spectroscopic patterns within complexes of one type of quinolinylaminophosphonate ligands indicates also the similar metal coordination patterns in their complexes, as described below. In all the complexes the less electronegative and coordinative poor phosphoryl oxygen towards palladium is not involved in metal bonding and is free to be involved in hydrogen bonding. Hydrogen bonding might be of interest for the biological activity of these complex compounds. It is presumed that the possibility of hydrogen bond formation might be important in the approaching and binding of metal ions to nucleic acid fragments.

3.2. X-ray studies

Molecular structures of complexes **1–4 and 6** are depicted in Figs. 2–5 and Figs. S1 and S3 in Supplementary data. Some interesting bond lengths and angles are listed in Table 2.

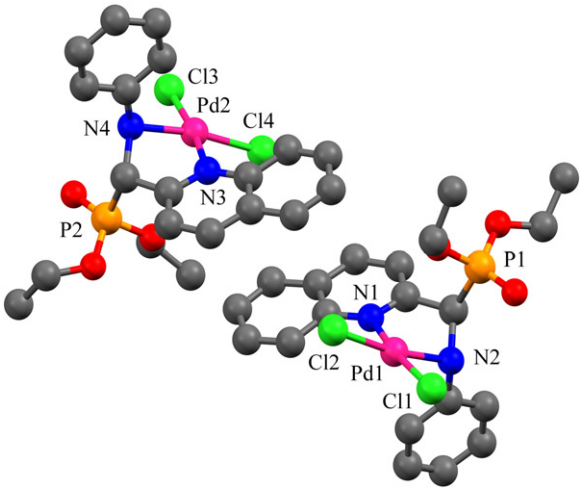

Fig. 2. Ball and stick view of both molecules in the asymmetric unit of the complex **1**. Alkyl chains reveal two orientations in the crystal. More populated orientation is shown. All hydrogen atoms are omitted for clarity. ORTEP view is given in Supplementary data (Fig. S1).

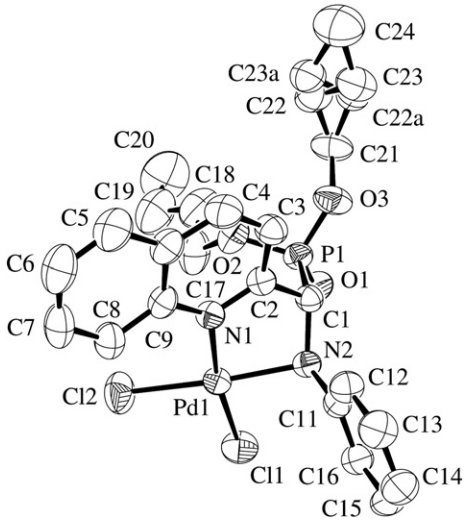

Fig. 4. Molecular structure of the complex **3**. Displacement ellipsoids are drawn at 50% probability level and all hydrogen atoms are omitted for clarity.

In crystal structures, strong N–H···O=P hydrogen bonds are the dominant intermolecular interaction (Table 3). Aminophosphonate groups of two molecules of opposite chiralities form centrosymmetric dimers, and in most of the described crystal structures, phosphoryl oxygen also forms the hydrogen bond with the neighbouring aromatic C–H donor functionality. Similar structural pattern was observed in other aminophosphonates, like diethyl (α-anilino-*N*-phenyl)phosphonate [46] and its recently published substituted derivatives [47]. Hydrogen bonds C–H···X (X=Cl, Br) also contribute to the crystal packing of complexes.

All chelate complexes (**1–4**) are square-planar and their characteristic structural feature is the five-membered chelate ring Pd–N(quinoline)–C–C–N(amino) that can be described either as twisted around the Pd–N(amino) bond (**1, 2, 2**·MeCN) or as the envelope on N(amino) atom (**3**) (Figs. 2–4 and Fig. S3). The chelate ring geometries observed in the similar chelate dichloride palladium(II) complexes with α-aminomethylpyridin-2-yl derivatives were analogous to ones described in this work [48–51]. Two symmetrically independent molecules of complex **1** are connected by the *π–π* interactions of quinoline rings (Table S1, Fig. S9). Complex **2** crystallizes from acetone (Fig. 3a) and as a monosolvate from MeCN (Fig. 3b). *π–π* interactions of quinoline rings are observed in both structures (Table S1, Fig. S10). The unusual feature of the crystal packing of the solvate is the absence of the characteristic N–H···O=P hydrogen bonding observed in all other structures described in this work. The interaction is blocked by positioning of the phosphoryl group in the hydrophobic pocket of the aryl and alkyl groups. Molecules of complex **2** in its acetonitrile solvate differ from those in the solvent free structure in the conformation of the phenyl ring and the ester groups. The difference can be assigned to the presence of the MeCN molecules in the structure of the solvate.

Complex **6** is square-planar with *trans* conformation and the palladium atom is situated in the crystallographic inversion centre (Fig. 5). Crystal packing motif involves chains of ten-membered rings $C(13)[R_2^2(10)]$ [52] formed by N–H···O=P hydrogen bonding of aminophosphonate moieties along the *c* axis (Fig. 6). Two aminophosphonate ligands are bonded to the palladium atom monodentately through the quinoline nitrogen atom similar to the complexes *trans*-$[PdL_2X_2]$ (X=Cl, Br; L=diethyl quinolin-2- (2-dqmp) or quinolin-8-ylmethylphosphonate (8-dqmp) [17,18], diethyl pyridin-3-ylmethylphosphonate [53], and pyridin-2- (2-pmOpe) and pyridin-4-ylmethylphosphate (4-pmOpe) [54]). Bond length Pd1–N1 is 2.033(3) Å and Pd1–Br1 is 2.4308(5) Å, similar to 2.064 Å and 2.435 Å, respectively, in *trans*-$[Pd(2\text{-dqmp})_2Br_2]$ [17]. The coordination sphere is almost an ideal square with the N1–Pd1–Br1 angle of 89.90(10)°. Twisting angle between the coordination plane and the plane of the bound quinoline ring is 74.88°. The similar values 80.63 and 79.00 were observed for *trans*-$[Pd(2\text{-dqmp})_2Cl_2]$ [17] and *trans*-$[Pd(2\text{-pmOpe})_2Cl_2]$ [54], respectively. Observed value can be rationalized by the need to accommodate present ethyl

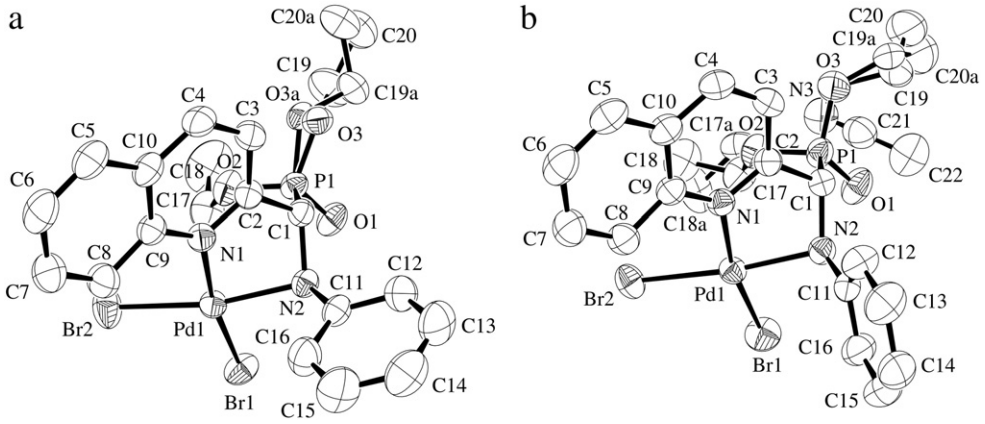

Fig. 3. Molecular structure of a) the complex **2** and b) its solvate **2**·MeCN. Displacement ellipsoids are drawn at 50% probability level and all hydrogen atoms are omitted for clarity.

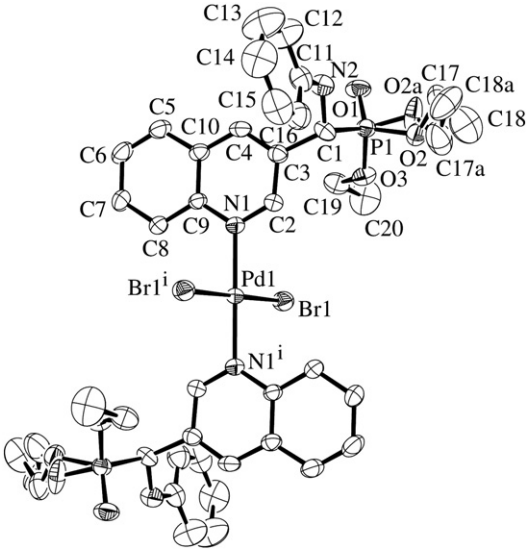

Fig. 5. Molecular structure of the complex **6**. Displacement ellipsoids are drawn at 30% probability level and all hydrogen atoms and EtOAc molecules are omitted for clarity. Palladium atom is positioned in the crystallographic inversion centre [0.5, 0.5, 0.5]. Unlabeled atoms are related by the symmetry operator i [1 − x, 1 − y, 1 − z].

acetate molecules and the steric hindrance of two large aminophosphonate ligands.

3.3. IR spectra

The IR frequencies associated with the main functional groups of the complexes are listed in the experimental section. When comparing the spectroscopic data of the complexes with those of the free ligands [34,35], marked changes may be noticed in the ligand bands arising from various modes of donor groups which are involved in bonding to palladium. The results obtained are in accordance with those obtained by X-ray structure analysis. The variation in position and intensity of absorptions in the region of 1615–1500 cm^{-1} associated with the stretching modes of the quinoline C=C and C=N bonds could be ascribed to π electronic redistribution in the heterocyclic ligand caused by metallation of the quinoline nitrogen. In this region occur also the NH deformation bands. The absorption of the NH stretching vibrations in the free ligands is found at about 3300 cm^{-1} as a strong (**L1–L4**) or medium band (**L5, L6**), indicating the existence of hydrogen bonding between the NH and P=O groups. In the complexes **1–4** this band is reduced in intensity and is shifted to lower frequencies by up to 100 cm^{-1} due to the bonding of the aniline group to the metal ion, while in the complexes **5–8** with only the quinoline nitrogen bonding it shows only a small higher frequency shift and an intensity decrease. In dipalladium complexes **9-12**, with both nitrogen donors bonding, in the ν(NH) region appears a broad absorption with maximum at lower frequency up to 40 cm^{-1} with respect to the free ligands and is broadened on its higher frequency side.

There are no great changes in the position of absorption bands of the phosphonic ester group as it is not involved in the metal coordination. The small variation in position of the ν(P=O) absorptions displayed in the 1260–1230 cm^{-1} region is arising from their sensitivity to the hydrogen bonding which may change the polarity of the phosphoryl oxygen atom and brings about the appearance of these bands at lower frequencies [55]. The spectra of all compounds show a great complexity within 1075-900 cm^{-1} where occur the stretching P-O-C and aliphatic C-C vibrations along with deformation modes of the alkyl ester groups and =CH vibrations of the quinoline and benzene rings [56].

The far-IR spectra (400–200 cm^{-1}) of complexes give insight into the metal–ligand vibrations which are very useful for determining the modes of ligand bonding. The position and the multiplicity of the palladium–halogen stretching bands could undoubtedly confirm either a *cis* or *trans* orientation of the terminal halogens in the complexes [57]. The two ν(Pd-X) bands are visible for the complexes **1–4** as expected for the *cis*-square-planar complexes in C_{2v} stereochemistry. In the complexes (**5–12**) one band characteristic for the *trans*-square-planar complexes in D_{2h} stereochemistry is found. It is worth noting that the presented spectroscopic data are in good agreement with those obtained for the corresponding types of the palladium complexes of quinolinylmethylphosphonates and anilinobenzylphosphonates [17,18,21,22,58].

Table 2
Selected bonds (Å) and angles (°) for complexes **1–3** and **6**. X=Cl or Br.

Bond	**1_1** [a]	**1_2** [a]	**2**	**2**·MeCN	**3**	**6**·2EtOAc
Pd1–X1	2.2778(12)	2.2663(15)	2.4079(4)	2.4137(3)	2.2704(8)	2.4308(5)
Pd1–*X2*	2.3002(10)	2.3039(14)	2.4297(4)	2.4305(3)	2.2937(9)	–
Pd1–N1	2.059(3)	2.056(3)	2.067(2)	2.0758(18)	2.100(2)	2.034(3)
Pd1–N2	2.069(3)	2.072(3)	2.076(2)	2.0703(19)	2.062(2)	–
Angle						
X1–Pd1–N1	–	–	–	–	–	89.90(11)
X1–Pd1–N2	92.02(8)	92.39(9)	92.61(7)	90.54(5)	89.78(7)	–
X1–Pd1–*X2*	91.61(4)	90.23(5)	92.03(1)	91.09(1)	89.05(3)	–
X2–Pd1–N1	96.74(9)	97.77(9)	96.22(7)	98.69(5)	100.26(7)	–
N1–Pd1–N2	79.25(11)	79.34(12)	78.54(9)	79.15(7)	80.96(9)	–

[a] Complex **1** comprises two molecules in an asymmetric unit. Data for both molecules are given. Molecule **1_1** contains Pd1 and molecule **1_2** contains Pd2. Accurate numbering of atoms in the molecule **1_2** is: Pd(n + 1), Cl(n + 2), N(n + 2), P(n + 1), O(n + 3), C(n + 20), where n is the numbering of analogous atom in the molecule **1_1**.

Table 3
Parameters for N–H···O=P hydrogen-bonding in the crystal structures of complexes **1–3** and **6**.

Complex		*d*(D–H)/Å	*d*(H···A)/Å	*d*(D–H···A)/Å	*α*(D–H···A)/°	Sym. op. *i*
1	N2–HN1···O4^i	0.91	2.15	2.965(4)	149	−1 + x, y, z
	N4–HN2···O1^i	0.91	2.11	2.916(4)	147	1 + x, y, z
2	N2–HN···O1^i	0.88(5)	2.09(4)	2.855(3)	145(5)	−x, −y, 1−z
3	N2–HN···O1^i	0.91	2.13	2.954(3)	150	1−x, −y, −z
6	N2–HN···O1^i	0.92(5)	2.12(5)	3.029(6)	169(5)	1−x, 1−y, 2−z

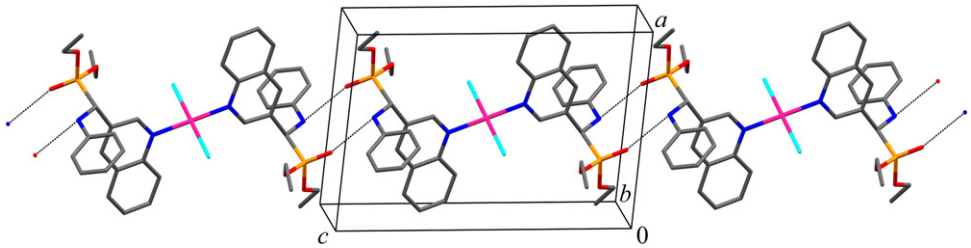

Fig. 6. Motif of the crystal structure of the complex **6** showing the C(13)[$R_2^2(10)$] chain of rings parallel to the [001] direction. Alkyl chains reveal two orientations in the crystal. More populated orientation is shown. Hydrogen atoms not participating in the N–H···O=P hydrogen-bonding are omitted for clarity.

3.4. NMR spectra

The ^{1}H, ^{13}C and ^{31}P NMR spectral studies of the complexes provide important structural information of these compounds. The complete ^{1}H and ^{13}C data obtained on the basis of one- and two-dimensional homo- and hetero-nuclear experiments are summarized in Supplementary data according to the numbering scheme shown in Fig. 1. The first point to be noted is that complexes retain their integrity in chloroform solution and that the results obtained are in agreement with those obtained by X-ray and IR analyses of complexes in the solid state. The spectral data for the free ligands provided a basis for interpreting the spectra of their complexes [34,35,56]. In all compounds two sets of separate H/C resonances have been observed for the diastereotopic alkyl ester groups of the $P(O)(OR)_2$ moiety. The spectral features are characterized by increased complexity arisen also from the H/C-phosphorus splitting. Proton of the PCH group appears either as a doublet with PH coupling or as a doublet of doublets due to simultaneous coupling with phosphorus (21.6–25.1 Hz) and NH proton (4.5–7.2 Hz). The NH proton appears as a broad singlet or a broad doublet, while in the **L4–L6** is visible a doublet of doublets, due to couplings with phosphorus and PCH proton. Carbon of the PCH group appears as a doublet with PC coupling of 140.7–151.7 Hz. The assignments of the aromatic H/C resonances were unambiguously ascertained by using a combination of the 1D and 2D multinuclear NMR analyses.

In the spectra of complexes, most of proton and carbon resonances show a certain high-frequency shift with respect to the free ligands. The decrease in the electron density in the heterocyclic aromatic ring caused by the metal coordination of the quinoline nitrogen to palladium atom and the proximity of the palladium atom which is known to be magnetically anisotropic [59], bring about deshielding of the atoms adjacent to the ligation sites. Thus, in the *N,N*-chelate complexes **1–4** the greatest downfield shift in the ^{1}H NMR spectra was observed for the aromatic H-8 (1.22–1.26 ppm) and H-4 (0.39–0.41 ppm) of the quinoline and H-4′ (0.52–0.53 ppm) and H-2′,6′ (0.27–0.28 ppm) of the aniline protons. Other aromatic protons resonances exhibit a smaller frequency shift which varies from 0.06 to 0.19 ppm. For the PCH proton a slight upfield shift of 0.19–0.21 ppm was observed, while the $POCH_2$ protons exhibit a downfield shift of 0.40–0.92 ppm. The other methylene protons as well methyl protons are shifted downfield by up to 0.25 ppm. In the ^{13}C NMR spectra, the pronounced high-frequency shifts were found for the C-2, C-4, C-2′,6′, C-4′, PCH and $POCH_2$ carbons of 3.57–4.31, 4.35–4.80, 5.86–6.12, 8.89–9.07, 12.79–13.21 and 3.79–4.19 ppm, respectively. The smaller downfield shifts exhibit C-5, C-8, C-10 and C-3′,5′ (up to 2.7 ppm), while for C-3, C-9 and C-1′ a slight upfield shielding was observed (up to 2.9 ppm).

As expected, in the spectra of complexes **5–8** the significant changes caused by complexation were observed only for the quinoline H/C resonances. The greatest downfield shift exhibit protons H-8 (1.79–1.88 ppm) and H-2 (0.54–0.56 ppm), the smaller one was found for H-7 (0.32–0.39 ppm) and H-4 (0.13–0.16 ppm), while all the other aromatic as well the non-aromatic PCH and alkyl protons exhibit very small downfield shift (up to 0.06 ppm). In the carbon resonances the greatest downfield shift show C-2 (4.23–4.68 ppm) and C-4 (2.56–2.86), the smaller one exhibit C-3 (1.47–1.58 ppm), C-6 (1.39–1.43 ppm), C-7 (1.61–1.95 ppm) and C-8 (0.37–1.03 ppm), while for C-9 an upfield shift (1.17–1.32 ppm) was observed. It is important to note that in the spectra of these complexes some H/C resonances show either broadening or multiplicity arising from the existence of more isomeric species in dynamic equilibrium in solution negligibly differing magnetically due to the restricted rotation around the Pd–N(quinoline) coordination bond. The similar spectroscopic feature was found for some palladium(II) and platinum(II) halide complexes of this type

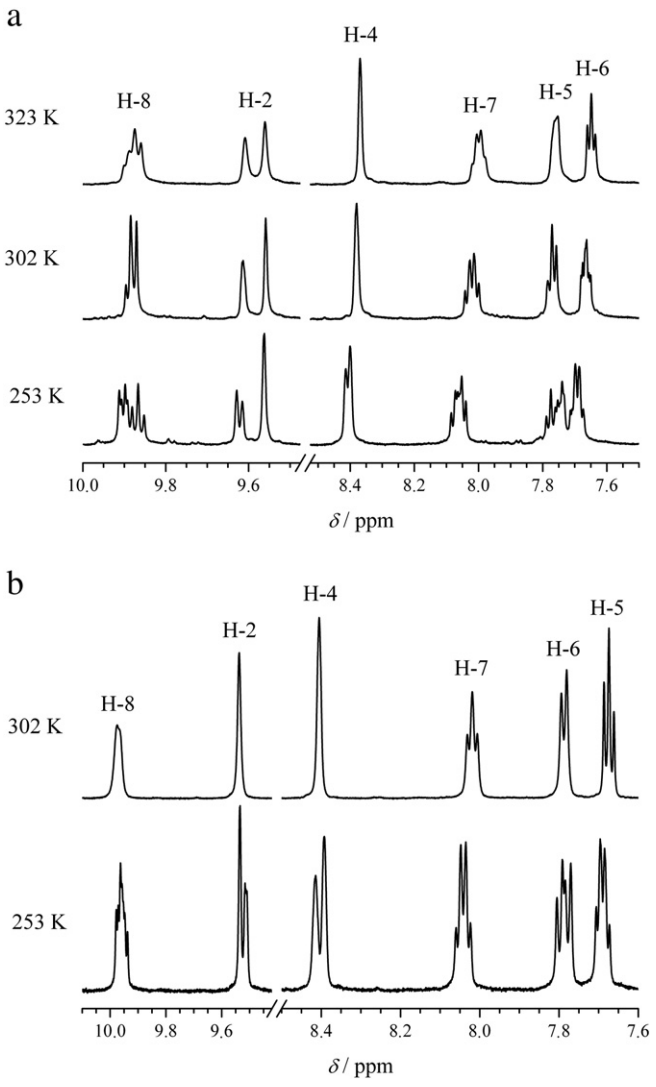

Fig. 7. Parts of ^{1}H NMR spectra of complexes a) **6** and b) **7** at various temperatures.

(*trans*-[ML_2X_2], M=Pd, Pt) with various quinoline and aniline derivatives [59–61]. In complex **5** two closely spaced signals are visible for the H-8, PCH, NH and C-2 resonances, while in complex **7** signals for the PCH, NH, C-2 and C-9 resonances are separated. The most of other H/C resonances exhibit only slight broadening. The situation is more complicated in the bromide complexes **6** and **8**, where for almost all H/C resonances the separated signals are visible. In the proton spectra resonances are doubled, but in the ^{13}C spectra of complex **6** even three sets of carbon signals are shown for the C-2, C-3, C-8 and PCH resonances, while in complex **8** only C-2 and PCH exhibit three separated signals. The existence of rotational isomers in these complexes, which distribution depends on both, the phosphonate (ethyl/butyl) and halogen (Cl/Br) ligand, was confirmed by variable temperature ^1H NMR measurements. By comparing the spectra at room temperature with those at 253 and 323 K, more pronounced changes were observed in the spectra recorded at lower temperature, where more signals of different intensities may be seen for almost all aromatic protons (Fig. 7). The connectivity from 2D NMR experiments enabled the assignments of H/C absorptions of all isomers and the most populated isomer could be ascribed to the less sterically hindered one.

The spectra of complexes **9–12** confirm their structure of having two terminal and one bridging ligand molecules (see Figs. 8 and 9). Either the broadening, presumably in the poorly soluble chloride complexes **9** and **11**, or the presence of two sets of signals in the ratio 2:1 were found for almost all H/C resonances in the corresponding bromide complexes **10** and **12**. The same signal ligands ratio was observed in the spectra of these complexes recorded at lower temperature (253 K, see Fig. 9). Similarly as in the complexes **5–8**, the greatest downfield shift is observed for the protons H-8 (1.62–1.82 ppm), H-2 (0.52–0.57 ppm) and H-7 (0.28–0.33 ppm) as well as the carbons C-2 (3.84–4.96 ppm) and C-4 (2.59–3.10 ppm). In general, the most of H/C resonances of the bridging ligand exhibit negligibly greater high-frequency shift with respect to that of the terminal ligand resonances. The exceptions are the NH and PCH proton resonances.

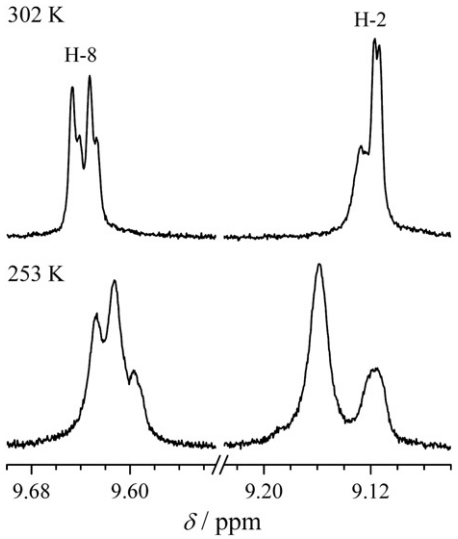

Fig. 9. Part of the ^1H NMR spectra of the complex **12** recorded at 302 and 253 K.

The valuable structural information about the complexes could be obtained by their ^{31}P NMR spectra, which data are given in Table 4 and partly presented in Fig. 10. All diester ligands **L1–L6** show a sharp absorption between 20.6 and 21.5 ppm. Due to the vicinity of the palladium atom in the chelate complexes **1–4** this absorption is shifted upfield by c.a. 6–7 ppm. As expected, more complicated spectral patterns are in the complexes with the 1:2 metal-to-ligand ratios, due to the presence of rotational isomers and their temperature redistribution. In spectra of the chloride complexes **5** and **7** at 302 K

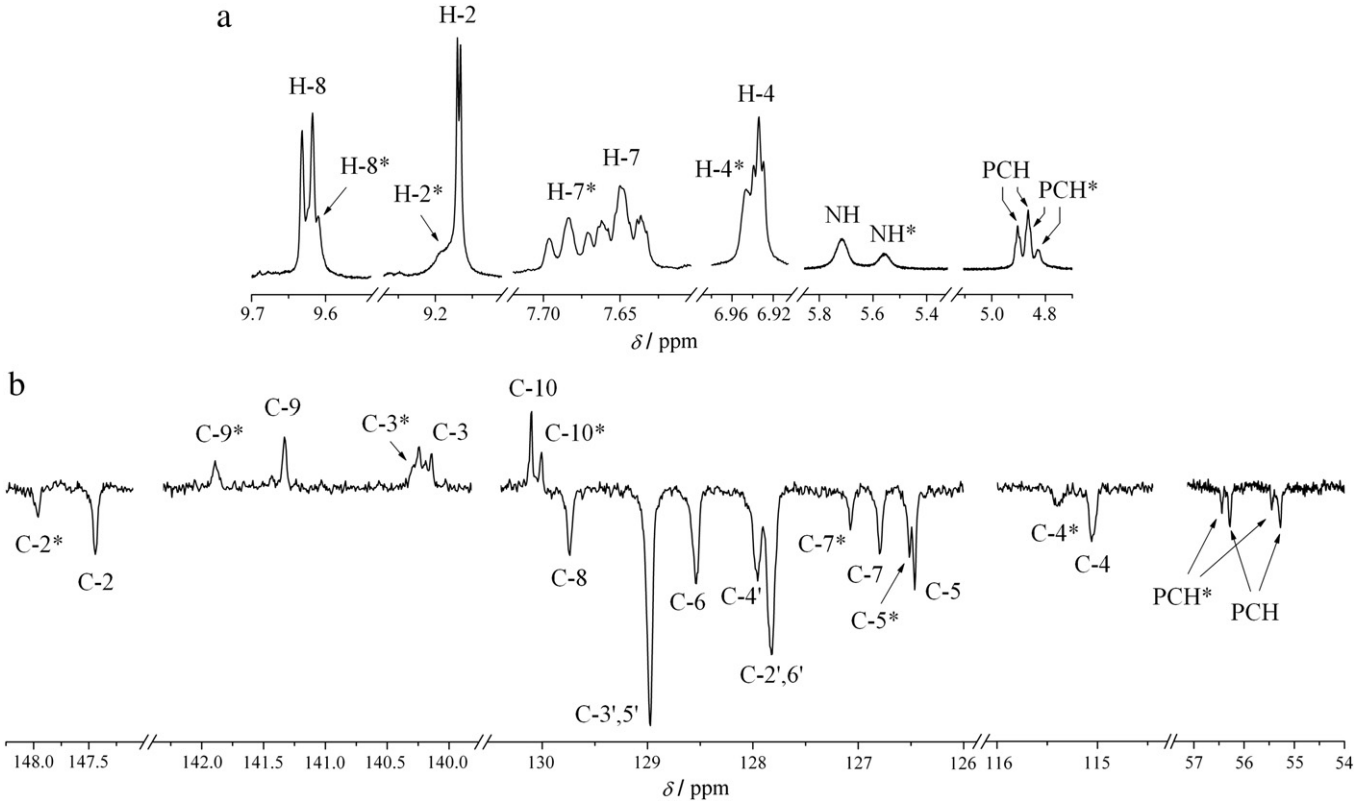

Fig. 8. Parts of a) ^1H and b) APT NMR spectra of the complex **10**. Signals of the bridging ligand are denoted with an asterisk (*).

Table 4
^{31}P NMR data (δ, ppm) for ligands **L1–L6** and their complexes **1–12**.[a]

	δ/ppm		δ/ppm		δ/ppm
L1	20.56	**1**	13.56	**2**	13.58
L2	20.46	**3**	14.24	**4**	14.19
L3	21.16	**5**	302 K: 20.44, 20.40 br (1:1.7) 253 K: 20.62, 20.51, 20.50, 20.41 (1:2.3:1.3) [b]	**6**	302 K: 20.84, 20.78, 20.75, 20.73 (1:1:1:1) 253 K: 20.57, 20.47, 20.43, 20.39 (2:1:3:1.3)
L4	21.18	**7**	302 K: 20.82 br 253 K: 20.56, 20.50, 20.46 (1.6:1:1)	**8**	302 K: 20.88, 20.85, 20.80, 20.79 (1:1.3) [c] 253 K: 20.63, 20.58, 20.51, 20.48 (1:1.6) [d]
L5	21.45	**9**	20.63,[e] 20.55 br (2:1)	**10**	20.66,[e] 20.62 br (2:1)
L6	21.39	**11**	21.33,[e] 21.27 br (2:1)	**12**	21.37, 21.33 br (2:1)

[a] Spectra recorded at 302 K unless stated otherwise. Ratio of signal intensities given in parentheses. br—broad.
[b] Partly overlapped signals at 20.51 and 20.50 ppm. Their joint intensity is 2.3.
[c] Partly overlapped signals at 20.88 and 20.85 ppm and those at 20.80 and 20.79 ppm. Ratio of joint intensities of pairs is 1:1.3.
[d] Partly overlapped signals at 20.63 and 20.58 ppm and those at 20.51 and 20.48 ppm. Ratio of joint intensities of pairs is 1:1.6.
[e] Signal of terminal ligands is broadened towards higher field due to the signal of the bridging ligand.

appear either two closely spaced absorptions at about 20.4 ppm (**5**) or a bit broader absorption at 20.8 ppm (**7**). At lower temperature (253 K) in these complexes are present four and three signals, respectively. In the corresponding bromide complexes **6** and **8**, both in the spectra at room and lower temperature, there are clearly visible four singlets between 20.7 and 20.9 ppm, but a different intensity ratio of signals and small chemical shift differences could be observed at various temperatures (Fig. 10b). In the spectra of complexes **9–12** there are two broadened singlets in the ratio 2:1 between 20.6 and 21.3 ppm arisen from two equivalent terminal and one bridging ligand molecules (Fig. 10c). In complexes **9–11** these absorptions are partly overlapped.

3.5. UV–vis spectra

The electronic absorption spectra of complexes obtained in chloroform solution in the 250–600 nm region show several overlapping bands, which complicate the assignation of the transitions involved. Quinolinyaminophosphonates alone show few intense band maxima between 270 and 350 nm due to π–π^* transitions, which is in accordance with the spectra of the substituted quinoline and aniline derivatives [19,62]. All palladium(II) complexes are diamagnetic with a square-planar geometry, for which three spin-allowed *d*–*d* transitions are expected, corresponding to transitions from the three lower lying *d*-levels to the empty $d_{x^2-y^2}$ orbitals [63]. The ground state is $^1A_{2g}$ and the excited states related to these transitions are $^1A_{2g}$, $^1B_{1g}$ and ^1E_g in order of increased energy. Overlapping of the strong absorptions from the charge-transfer or intraligand π–π^* transitions prevents the observation and detection of the expected bands [19,21]. The most prominent absorption is around 400 (**1–4**), 324 (**5–8**) and 368 (**9–12**) nm, respectively, which could be ascribed to the metal-to-ligand charge-transfer transitions. The relatively dark colour of complexes **1–4** indicates strong charge-transfer absorptions originating in the ultraviolet and trailing off into the visible region, while the relatively pale colour of the other complexes indicates that the quinoline ligand has a low ligand field strength in forming these complexes. In addition, the intensity of absorption bands is slightly higher for the bromide complexes than their chloride analogues, which could be ascribed to the increased ligand participation in the occupied MO-levels, derived mainly from the metal *d*-levels.

3.6. Mass spectra

The structure of the complexes was also supported by the mass spectra carried out under positive-ion ESI conditions, but here are given only the major structurally informative data for the complexes **9–12**, as for this type of palladium complexes we could not grow crystals for X-ray analysis. The mass spectrometric behaviour and fragmentation pathways of the free ligands and their complexes studied by collisional experiments on the ESI-generated species (ESI MS^n) will be published in detail elsewhere. In the ESI spectra (positive ions) all the complexes show the presence of the molecular ion as sodium adduct $[M+Na]^+$ supporting the 1:1, 1:2 and 2:3 metal-to-ligand ratio in complexes **1–4, 5–8 and 9–12**, respectively. Formation of sodiated molecular ions, very often present instead of the corresponding protonated molecular ions, is the normal feature in the ESI MS spectra of compounds investigated under positive ion electrospray ionization conditions. In the case of complexes **9–12** the important diagnostic fragment ions are those obtained by losses of one ligand molecule as well as $PdLX_2$, PdL_2X_2, PdL_2X_3 and $Pd_2L_2X_4$ from the sodiated molecular ion finally leading to the sodium adduct of the free ligand $[L+Na]^+$.

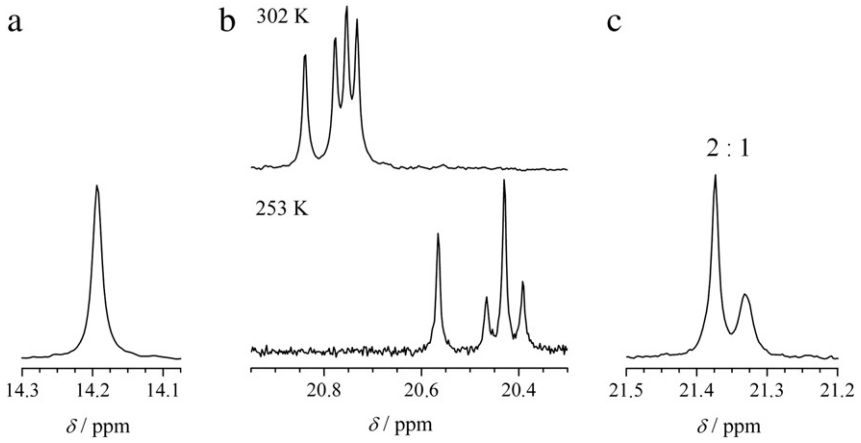

Fig. 10. $^{31}P\{^1H\}$ NMR spectra of complexes a) **4**, b) **6** and c) **12**.

Table 5
Inhibitory effects of palladium complexes **1–12** on the growth of human tumor cell lines.

	IC_{50} (μM)				
Complex	SW 620	H 460	MCF-7	HCT 116	MOLT-4
1	>100	92 ± 3	>100	61 ± 7	74 ± 26
2	89 ± 7	83 ± 12	85 ± 12	70 ± 23	>100
3	15 ± 2	15 ± 0.3	18 ± 0.1	10 ± 7	19 ± 4
4	15 ± 0.2	13 ± 0.3	14 ± 1	11 ± 7	21 ± 0.6
5	31 ± 27	36 ± 21	≥100	20 ± 2	46 ± 25
6	31 ± 13	42 ± 11	39 ± 19	24 ± 0.1	13 ± 3
7	12 ± 0.6	4 ± 2	10 ± 1	4 ± 0.1	17 ± 12
8	14 ± 2	7 ± 0.1	9 ± 4	4 ± 0.2	20 ± 9
9	5 ± 0.7	17 ± 1	11 ± 2	5 ± 0.5	8 ± 5
10	15 ± 0.5	18 ± 1	13 ± 2	13 ± 3	13 ± 0.6
11	3 ± 0.5	3 ± 0.4	2 ± 0.6	2 ± 0.6	8 ± 4
12	4 ± 0.1	3 ± 0.2	6 ± 5	3 ± 0.4	8 ± 6
Cisplatin	7 ± 4	0.3 ± 0.02	10 ± 5	7 ± 3	0.2 ± 0.04

3.7. Antitumor activity

The antiproliferative activity of the complexes was determined *in vitro* on five human tumor cell lines derived from four cancer types: colon carcinoma (SW 620 and HCT 116), lung carcinoma (H 460), breast carcinoma (MCF-7) and T-lymphoblast leukemia cells (MOLT-4). The results, expressed as concentration of the complex required to inhibit the tumor cell growth by 50% (IC_{50}), are summarized in Table 5 and the concentration–response profiles for the chloride complexes are given in Fig. 11.

It was shown that complexes possess differential antiproliferative activity against the examined cell lines at the tested concentration range (0.01–100 μM). In general, it was shown that there is no significant difference in sensitivity between the five tumor cell lines, neither between the corresponding chloride and bromide complexes. Only HCT 116 cell was slightly more sensitive than the other cell lines. This is somewhat in contrast to the sensitivity of these five cell lines to cisplatin; for example cell lines H 460 and MOLT-4 show more pronounced sensitivity to this chemotherapeutic. Also, tetrachlorido complex **9** was slightly more active with respect to its tetrabromido analogue **10**. Most importantly, complexes of dibutyl esters in all three types of complexes are significantly more effective than those of diethyl esters, which may be partly ascribed to the greater lipophilicity and membrane permeability of the former complexes. The lipophilicity of the complexes increases from diethyl to dibutyl derivatives and may facilitate transport through the cellular membranes [64]. Among complexes of butyl esters the most significant activity at low micromolar range, which is comparable to the activity of the reference compound cisplatin, show dipalladium complexes **11**

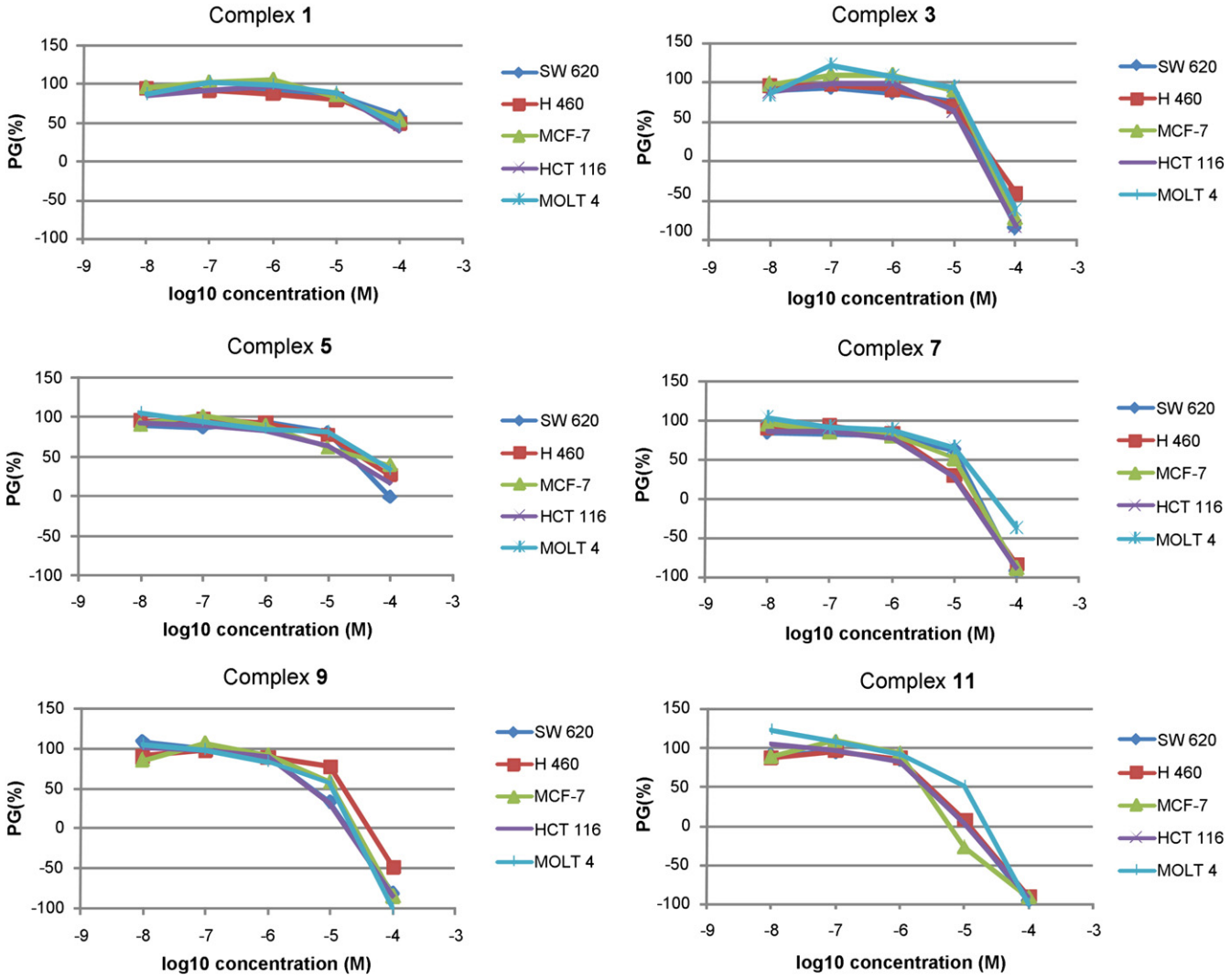

Fig. 11. Concentration–response profiles for the chloride complexes (**1, 3, 5, 7, 9, 11**) tested on various human tumor-cell lines *in vitro*. The cells were treated with the complexes at different concentrations, and the percentage of growth (PG) was calculated. Each point represents a mean value of four parallel samples in three individual experiments.

and **12** (IC_{50} 2–8 μM), somewhat less active are mononuclear complexes **7** and **8** (IC_{50} 4–20 μM) and **3** and **4** (IC_{50} 11–21 μM) with *trans*- and *cis*-configuration, respectively. There are much greater variations in response between complexes of diethyl esters. Thus, while dipalladium complexes **9** and **10** show pronounced activity (IC_{50} 5–18 μM), mononuclear complexes display either modest activity as in the case of complexes **5** and **6** (IC_{50} 13–46 μM), with one exception of complex **5** on MCF-7 cells with IC_{50}>100, or have extremely modest antiproliferative activity as complexes **1** and **2** (IC_{50}>60 μM). It is important to note that free dibutyl esters were found to show extremely low, if any, antitumor activity in MOLT-4 cells with IC_{50} value between >100 and >400 μM [34], and therefore, it may be presumed that the free ligands do not participate a lot in activity of the complexes. Furthermore, it is interesting to compare the results of the *in vitro* assays on the same tumor cell line related to the palladium dihalide complexes of diethyl quinolin-2- and quinolin-8-ylmethylphosphonates [19,24]. *Cis*-complexes with 1:1 metal-to-ligand ratio of diethyl quinolin-2-ylmethylphosphonate are more active than the *cis*-complexes **1** and **2**, while those with 1:2 ratio and *trans*-configuration are less active than complexes **5** and **6** [19]. On the other side, *trans*-complexes of quinolin-8-ylmethylphosphonate show significant antitumor activity with IC_{50}<10 μM. These findings support the general assumption that the relationship between structure and activity is extremely complex and depend on a lot of factors. Thus, the differences in lability between the halide groups in different type of complexes may alter the biochemical properties of the complexes, as the breaking ability of the Pd–halogen bond is presumed to be the crucial step in complex reaction with DNA strands. In addition, the introduction of the second metal binding unit, which can also interfere with nucleobases of DNA, may enhance the cytotoxic effect [65]. This is in accordance with finding that dinuclear complexes **9–12** show the higher activity with respect to mononuclear complexes **1–8**.

3.8. Antimicrobial activity

The three different series of complexes **1–4, 5–8 and 9–12** were tested for their *in vitro* antimicrobial activity against a large number of standard microorganisms representative of Gram positive and Gram negative bacteria, yeasts and moulds. The starting ligands **L1–L6** and palladium salts $Na_2[PdCl_4]$ and $Na_2[PdBr_4]$ were also included for a comparison.

Most of the tested compounds are devoid of antibacterial and antifungal properties up the concentration of 200 μg/mL. Only a weak inhibition could be detected towards some Gram positive bacteria with MIC values of 200 μg/mL. In this regard, **L3** and **L6** ligands and complex **11** inhibit the growth of *B. thuringiensis* var. *kurstaki* and a similar behaviour is shown by ligand **L6** and complex **9** against *B. megaterium* and *S. epidermidis*. These compounds act as bacteriostatic agents, exhibiting minimal bactericidal concentrations higher than the corresponding MICs (MBCs >200 μg/mL).

Although the low degree of antibacterial activity prevents from establishing extensive structure–activity relationships, it is interesting to observe that both the active ligands **L3** and **L6** are 3-substituted quinolines and that only dinuclear tetrachlorodipalladium complexes (compounds **9** and **11**) exhibited antibacterial properties. Furthermore, the different lipophilicity of the ethyl and butyl substituents at the phosphonate moiety does not significantly affect the inhibition of the growth of tested microorganisms.

4. Conclusion

A series of novel palladium(II) chloride and bromide complexes with three types of quinolinylaminophosphonates have been synthesized and structurally characterized. All organophosphorus ligands contain three potential donor atoms, quinoline nitrogen, amino nitrogen and phosphoryl oxygen, but their coordination behaviour towards palladium(II) ion is different. In complexes either quinoline or both quinoline and amino nitrogens are involved in metal(s) bonding forming mononuclear dihalide adducts either with *cis*- or *trans*-configuration as well as dinuclear tetrahalide complexes. Phosphoryl oxygen is not coordinated and is free to be involved in hydrogen bonding, which is the main feature of crystal structures of complexes. The stereochemistry of the complexes, the nature of metal–ligand binding and hydrogen bond interactions are investigated by spectroscopy and X-ray structure analysis. Biological properties of complexes were examined by screening of their ability to inhibit the cancer growth *in vitro* in a panel of human tumor cell lines and their antimicrobial activity in a wide spectrum of bacterial and fungal strains. While no specific antimicrobial effects of both the free organophosphorus ligands and their palladium(II) halide complexes were noted, the majority of complexes demonstrated cytostatic activity, which was especially pronounced in the case of dipalladium tetrahalide complexes with IC_{50}<10 μM. It may be concluded that palladium complexes of investigated quinolinylaminophosphonates represent an interesting class of new complex compounds from the viewpoint of their physicochemical, structural and biological properties.

Supplementary data associated with this article, including additional crystallographic and spectroscopic data along with the results of antimicrobial screening, can be found in the online version at doi:10.1016/j.jinorgbio.2011.03.011.

Abbreviations

M.p.	Melting point
Decomp.	Decomposition
DMF	Dimethylformamide
MTT	Tetrazolium [3-(4,5-dimethylthiazol-2-yl)-2,5-diphenyltetrazolium bromide]
MO	Molecular Orbital
MW	Microwave
UV–vis	Ultraviolet–visible
APT	Attached Proton Test
COSY	COrrelation SpectroscopY
HMQC	Heteronuclear Multiple Quantum Coherence
HMBC	Heteronuclear Multiple Bond Correlation
ESI MS	ElectroSpray Ionization Mass Spectroscopy
ORTEP	Oak Ridge Thermal Ellipsoid Plot
CCD	Charge-Coupled Device
PG	Percentage of Growth
OD	Optical Density
IC_{50}	Concentration necessary for 50% of inhibition of cell growth
MIC	Minimal inhibitory concentration
MBC	Minimum bactericidal concentration
SW 620	Human colorectal adenocarcinoma cell line
H 460	Human large cell lung cancer cell line
MCF-7	Human breast adenocarcinoma cell line
HCT 116	Human colon cancer cell line
MOLT-4	Human acute lymphoblastic leukemia cell line

Acknowledgements

The financial support of the Croatian Ministry of Science, Education and Sports (grant Nos. 098-0982915-2950, 098-1191344-2943 and 098-0982464-2514) is gratefully acknowledged. The authors would like to thank B. Sc. S. Roca and Mr. Sc. Ž. Marinić for recording the NMR spectra and Dr. L. Šuman for screening the antitumor assays.

References

[1] Cisplatin: Chemistry and Biochemistry of a Leading Anticancer Drug, in: B. Lippert (Ed.), Wiley–VCH, Weinheim, 1999.
[2] P.J. O'Dwyer, P. Stevenson, S.W. Johnson, Clinical status of cisplatin, carboplatin, and other platinum-based antitumor drugs, in: B. Lippert (Ed.), Cisplatin: Chemistry and Biochemistry of a Leading Anticancer Drug, Verlag Helvetica Chimica Acta, Zurich, 1999, pp. 31–72.
[3] G. Natile, M. Coluccia, Coord. Chem. Rev. 216–217 (2001) 383–410.
[4] G. Momekov, A. Bakalova, M. Karaivanova, Curr. Med. Chem. 12 (2005) 2177–2191.
[5] S. van Zutphen, J. Reedijk, Coord. Chem. Rev. 249 (2005) 2845–2853.
[6] J. Reedijk, Eur. J. Inorg. Chem. (2009) 1301–1312, and references therein.
[7] S.M. Aris, N.P. Farrell, Eur. J. Inorg. Chem. (2009) 1293–1302.
[8] E. Alessio, G. Menstroni, A. Bergamo, G. Sava, Curr. Top. Med. Chem. 4 (2004) 1525–1535.
[9] G. Zhao, H. Lin, Curr. Med. Chem. Anticancer Agents 5 (2005) 137–147.
[10] M.A. Jakupec, M. Galanski, V.B. Arion, C.G. Hartinger, B.K. Kepler, Dalton Trans. (2008) 183–194.
[11] A. Alama, B. Tasso, F. Novelli, F. Sparatore, Drug Discov. Today 14 (2009) 500–508.
[12] A. Casini, C. Hartinger, C. Gabbiani, E. Mini, P.J. Dyson, B.K. Keppler, L. Messori, J. Inorg. Biochem. 102 (2008) 564–575.
[13] P. Kafarski, B. Lejczak, Aminophosphonic and aminophosphinic acids, in: V.P. Kukhar, H.R. Hudson (Eds.), Chemistry and Biological Activity, John Wiley & Sons, Chichester, 2000, pp. 407–442.
[14] H. Kozlowski, A. Pusino, J. Swiatek, J. Spychala, T. Glowiak, G. Micera, C. Gessa, J. Agric, Food Chem. 38 (1990) 1989–1992.
[15] P. Kafarski, B. Lejczak, Curr. Med. Chem. Anticancer Agents 1 (2001) 301–312.
[16] T. Klenner, P. Valenzuela-Paz, F. Amelung, H. Münch, H. Zahn, B.K. Keppler, H. Blum, Platinum phosphonato complexes with particular activity against bone malignancies. An evaluation of an experimental model highly predictive for the clinical situation, in: B.K. Keppler (Ed.), Metal Complexes in Cancer Chemotherapy, VCH, Weinheim, 1993, pp. 85–127.
[17] Lj. Tušek-Božić, I. Matijašić, G. Bocelli, G. Calestani, A. Furlani, V. Scarcia, A. Papaioannou, J. Chem. Soc. Dalton. Trans. (1991) 195–201.
[18] Lj. Tušek-Božić, I. Matijašić, G. Bocelli, G. Sgarabotto, A. Furlani, V. Scarcia, A. Papaioannou, Inorg. Chim. Acta 185 (1991) 229–237.
[19] Lj. Tušek-Božić, A. Furlani, V. Scarcia, E. De Clercq, J. Balzarini, J. Inorg. Biochem. 72 (1998) 201–210.
[20] Lj. Tušek-Božić, F. Frausin, V. Scarcia, A. Furlani, J. Inorg. Biochem. 95 (2003) 259–269.
[21] Lj. Tušek-Božić, M. Juribašić, P. Traldi, V. Scarcia, A. Furlani, Polyhedron 27 (2008) 1317–1328.
[22] M. Ćurić, Lj. Tušek-Božić, D. Vikić-Topić, V. Scarcia, A. Furlani, J. Balzarini, E. De Clercq, J. Inorg. Biochem. 63 (1996) 125–142.
[23] Lj. Tušek-Božić, M. Komac, M. Ćurić, A. Lyčka, M. D'Alpaos, V. Scarcia, A. Furlani, Polyhedron 19 (2000) 937–948.
[24] Lj. Tušek-Božić, V. Cmrečki, J. Balzarini, E. De Clercq, Lett. Drug Des. Discov. 3 (2006) 528–533.
[25] E. Budzisz, U. Krajewska, M. Rozalski, A. Szulawska, M. Czyz, B. Nawrot, Eur. J. Pharmacol. 502 (2004) 59–65.
[26] J. Kuduk-Jaworska, A. Puszko, M. Kibiak, M. Pelczynska, J. Inorg. Biochem. 98 (2004) 1447–1456.
[27] D. Kovala-Demertzi, A. Bocarelli, M.A. Demertzis, M. Coluccia, Chemotherapy 53 (2007) 148–152.
[28] G. Faraglia, D. Fregona, S. Sitran, L. Giovagnini, C. Marzano, F. Baccichetti, U. Casellato, R. Graziani, J. Inorg. Biochem. 83 (2001) 31–40.
[29] L. Giovagnini, L. Ronconi, D. Aldinucci, D. Lorenzon, S. Sitran, D. Fregona, J. Med. Chem. 48 (2005) 1588–1595.
[30] A. Garoufis, S.K. Hadjikakou, N. Hadjiliadis, Coord. Chem. Rev. 253 (2009) 1384–1397, and references therein.
[31] S. Kumar, S. Bawa, H. Gupta, Mini Reviews Med. Chem. 9 (2009) 1648–1654.
[32] F. O'Donnell, T.J.P. Smyth, V.N. Ramachandran, W.F. Smyth, Int. J. Antimicrob. Agents 35 (2010) 30–38.
[33] A.H. Kategaonkar, R.U. Pokalwar, S.S. Sonar, V.U. Gawali, B.B. Shingate, M.S. Shingare, Eur. J. Med. Chem. 45 (2010) 1128–1132.
[34] Lj. Tušek-Božić, M. Juribašić, M. Komac, V. Cmrečki, I. Zrinski, J. Balzarini, E. De Clercq, Lett. Org. Chem. 4 (2007) 332–338.
[35] M. Juribašić, L. Stella, Ž. Marinić, M. Vinković, Lj. Tušek-Božić, Lett. Org. Chem. 6 (2009) 11–16.
[36] M.J.A. Jungbauer, C. Curran, Spectrochim. Acta 21 (1965) 641–648.
[37] A.K. Majumdar, S.P. Bag, Frasenius Zeit. Analyt. Chem. 165 (1959) 247–250.
[38] CrysAlis PRO, Oxford Diffraction Ltd, Oxford, U. K, 2007.
[39] G.M. Sheldrick, Acta Crystallogr. A64 (2008) 112–122.
[40] A.L. Spek, J. Appl. Crystallogr. 36 (2003) 7–13.
[41] L.J. Farrugia, J. Appl. Crystallogr. 30 (1997) 565–566.
[42] P. McCabe, E. Pidcock, G.P. Shields, R. Taylor, M. Towler, C.F. Macrae, P.R. Edgington, J. Van de Streek, J. Appl. Crystallogr. 39 (2006) 453–457.
[43] M.R. Boyd, K.D. Pauli, Drug Dev. Res. 34 (1995) 91–109.
[44] T. Mossman, Immunol. Meth. 65 (1983) 55–63.
[45] J.H. Jorgensen, J.D. Turnidge, in: P.R. Murray, E.J. Baron, M.A. Pfaller, F.C. Tenover, R.H. Yolken (Eds.), Manual of Clinical Microbiology, American Society for Microbiology, Washington, DC, 1999, pp. 1526–1554 and 1640–1652.
[46] Z. Ružić-Toroš, B. Kojić-Prodić, M. Šljukić, Acta Crystallogr. B34 (1978) 3110–3113.
[47] C. Li, B. Song, K. Yan, G. Xu, D. Hu, S. Yang, L. Jin, W. Xue, P. Lu, Molecules 12 (2007) 163–172, and references therein.
[48] V. Diez, J.V. Cuevas, G. Garcia-Herbosa, G. Aullon, J.P.H. Charmant, A. Carbayo, A. Munoz, Inorg. Chem. 46 (2007) 568–578.
[49] S. Doherty, J.G. Knight, T.H. Scanian, M.R.J. Elsegood, W. Clegg, J. Organomet. Chem. 650 (2002) 231–248.
[50] V. Terrasson, D. Prim, J. Marrot, Eur. J. Inorg. Chem. (2008) 2739–2745.
[51] C.-Y. Liao, K.-T. Chan, C.-Y. Tu, Y.-W. Chang, C.-H. Hu, H.M. Lee, Chem. Eur. J. 15 (2009) 405–417.
[52] J. Bernstein, R.E. Davis, L. Shimoni, N.-L. Chang, Angew. Chem. Int. Ed. 34 (1995) 1555–1573.
[53] A.L. Spek, private commun, 2000.
[54] U. Kalinowska, L. Chęcińska, M. Małecka, A. Erxleben, B. Lippert, J. Ochocki, Inorg. Chim. Acta 358 (2005) 2464–2472.
[55] L.C. Thomas, Interpretation of Infrared Spectra of Organophosphorus Compounds, Plenum Press, New York, 1974.
[56] M. Juribašić, Lj. Tušek-Božić, J. Mol. Struct. 924–926 (2009) 66–72.
[57] K. Nakamoto, Infrared and Raman Spectra of Inorganic and Coordination Compounds, Part B: Applications in Coordination Organometallic and Bioinorganic Chemistry, 5th Ed, Wiley–Interscience, 1997.
[58] Lj. Tušek-Božić, M. D'Alpaos, Polyhedron 17 (1998) 1481–1493.
[59] A. Albinati, P.S. Pregosin, F. Wombacher, Inorg. Chem. 29 (1990) 1812–1817.
[60] Lj. Tušek-Božić, M. Ćurić, D. Vikić-Topić, A. Lyčka, Collect. Czech. Chem. Commun. 62 (1997) 1888–1904.
[61] L.A. Silks III, J. Peng, J.D. Odom, B. Dunlap, J. Org. Chem. 56 (1991) 6733–6736.
[62] H.H. Jaffe, M. Orchin, Theory and Applications of Ultraviolet Spectroscopy, J. Wiley, New York, 1962.
[63] S.E. Livingstone, The Chemistry of Ruthenium, Rhodium, Palladium, Osmium, Iridium and Platinum Complexes, Pergamon Press, Oxford, 1973.
[64] J.P. Souchard, T.T.B. Ha, S. Cros, N.P. Johnson, J. Med. Chem. 34 (1991) 863–864.
[65] S. Fakih, W.C. Tung, D. Eierhoff, C. Mock, B. Krebs, Z. Anorg. Allg. Chem. 631 (2005) 1397–1402.